UCRL - 76269
PREPRINT
Conf-741213--18

LAWRENCE LIVERMORE LABORATORY
University of California/Livermore, California



# PROGNOSIS FOR HIGH-Z SEMICONDUCTOR DETECTORS

S. P. Swierkowski and G. A. Armantrout

December 6, 1974



This Paper was Prepared for Submittal to
IEEE Transactions on Nuclear Science

# PROGNOSIS FOR HIGH-Z SEMICONDUCTOR DETECTORS*

S. P. SWIERKOWSKI AND G. A. ARMANTROUT
Lawrence Livermore Laboratory, University of Califor a
Livermore, California 94550

## Abstract

Considerable interest has been generated recently in the use of high-Z semiconductors for x-ray spectroscopy. To aid in this study, a Monte-Carlo computational model has been used to simulate x-ray spectral response in semiconductor detectors. The model employs one-dimensional charge collection in an arbitrary electric field profile and includes trapping and electronics system effects. Spectra are calculated for several materials, including $HgI_2$ and CdTe, and are compared to experimental results.

## Introduction

Recent work[1-7] on high-Z, ambient operating temperature semiconductor detector materials, particularly $HgI_2$ and CdTe, has indicated the importance that charge transport and trapping effects will have in limiting detector performance. The ambient temperature requirement implies that the bandgap should be ≥ 1.5 eV to reduce intrinsic detector noise to an acceptable level. Since a general inverse dependence of mobility upon bandgap exists,[8] limitations caused by low carrier mobilities may be expected. A most useful figure of merit for charge transport is the mean length before trapping ($L_e$ or $L_h$) given by the product of the mobility ($\mu$), trapping time ($\tau$) and electric field (E). For example, in germanium at 77°K, $L_e \cong L_h \cong 10^4$ cm which is much greater than the detector length, DL ≅ 2 cm. By way of contrast, measurements on $HgI_2$ at 300°K (perpendicular to the natural cleavage plane) indicate $L_e \cong 1$ cm and $L_h \cong 0.1$ cm compared to a typical detector thickness of DL ≅ 0.1 cm. The combination of low mobilities and short carrier lifetimes results in trapping lengths comparable to detector lengths and makes the prediction of detector system performance nontrivial but may account for many observed spectral effects in wide bandgap semiconductors.

Several analytical models[9-11] have been described to predict the effect of transport properties on spectral peak shape and charge collection efficiency. The analytical nature of these models gives one a feeling for the relevant parameters and their effects; however, they do not include nonanalytical electric field profiles, Compton absorption, x-ray and electron escape, amplifier noise, and pulse shaping time-constant effects on the total detector system spectral response. This last effect, for example, is of major importance in $HgI_2$ where the transit time for holes parallel to the c axis across a one millimeter thick detector is typically several microseconds. A Monte-Carlo computer code was written that would accommodate the above effects and predict x-ray and low energy x-ray spectra for a given source. This model is useful for a variety of applications such as the ability to predict the upper useful size limit of a given crystal before it is grown to that size by using the transport properties measured on the best available small crystals. It is also of assistance in understanding the effects on spectral performance caused by dead layers, nonuniform electric fields and polarization, trapping, detector geometry, and electronics system noise and time constants. For well characterized materials such as germanium, the code will be useful for optimizing the detector geometry, source-detector orientation, and to estimate photopeak detection in low count rate situations.

## Computational Model

The model is naturally divided into two major parts. The first part is the energy (or charge) deposition and the second part is the charge transport and system electronics. This division is also computationally efficient since a given set of initial charge distributions may be stored and used several times with different transport and electronics parameters. Desirable physical processes for the energy deposition part include the photoelectric effect, Compton scattering, pair production, ionization energy loss, fluorescence, bremsstrahlung, knock-on electrons, and Auger electron emmission. ETRAN and SANDYL[12,13] are Monte-Carlo codes that incorporate the above effects; they are currently being adapted for use with the charge transport part of the model. The preliminary results that follow use only the photoelectric absorption process and do not include electron escape. The range of photon energies is such that the photoelectric cross sections are approximately ten times that for Compton. In addition, the assumption of point interactions and no electron escape is a reasonable approximation in this energy range.

The transport part of the model is one-dimensional. The detector is divided into a series of slabs perpendicular to the electric field. The spatial and temporal history of the electron and hole charges in each slab are followed separately until the charge reaches an electrode or is completely trapped. The incremental induced charge on the electrodes is followed temporally for all charge groups. When all charge groups have stopped drifting, the final signal, which is the induced charge on the electrodes as a function of time, is computed. Three basic approximations are made. First, the initial charge distribution is assumed to have a negligible perturbation on the internal electric field of the device. This is a good approximation for photon energies less than a few MeV at typical spectrometer count rates. Second, only single photon events are allowed. Third, detrapping is not included in the model. For most applications, the detrapping time is much greater than the shaping time, thus the effect is negligible.

Statistical fluctuations enter into the calculations in several places. First, the energy of the

* This work performed under the auspices of the U.S. Atomic Energy Commission.

photon is selected randomly from the input spectrum according to its weight. After the photon absorption processes are complete, the entire resulting electron-hole pair distribution is subjected to a Gaussian fluctuation modified by a Fano factor. Each charge group is repeatedly allowed to drift an amount $\Delta x$, the independent variable. The elapsed time, the dependent variable, is computed using the average electric field and then the subsequent amount of trapped charge is calculated and is subjected to a Gaussian fluctuation. The average amount of charge in the group in drifting the amount $\Delta x$ is used to calculate the incremental induced signal. The incremental induced charge $\Delta Q$ induced on the detector capacitance by a charge $\bar{q}$ moving along the electric field is given by

$$V \Delta Q = \bar{q} \vec{E}(x) \cdot \vec{\Delta x} \qquad (1)$$

where V is the potential across the detector. The final charge pulse as a function of time is then multiplied by a filter function to account for the integration and differentiation time constants. Finally, the resulting peak signal is subjected to a Gaussian noise fluctuation to simulate electronic noise sources.

## Computed and Experimental Results

Initial results were calculated for charge collection along the c axis in $HgI_2$. The mobilities used, $\mu_E$ = 96 $cm^2$/V-sec and $\mu_H$ = 3 $cm^2$/V-sec (denoted by UE and UH in the computer generated plots) are average reported values.[4-7] The trapping times, in seconds, for electrons and holes are denoted by TE and TH respectively. In addition, the detector length in cm, DL, and the detector bias in volts, V, are shown in the plots. The alphanumeric ID line has the detector material, the source spectrum, and the data filename preceded by a sign which indicates the polarity of the electrode the source is incident upon. If the filename is succeeded by an "E", a nonuniform electric field was used. In Figures 1-7 and 11-12, the integration and differention time constants are $\tau_I = \tau_D = 3$ μsec and the electronic noise is 1.5 keV FWHM referred to $HgI_2$.

Figures 1-5 show the effect of changing only the detector length, DL, while holding the electric field and all other parameters constant. The average penetration depth ($\bar{x}$) for the 59.54 keV x-ray after normalization by the detector length is also shown in the figures. The shoulder effect on the 59.54 keV x-ray photopeak in Figure 2 has also been experimentally observed; the lower edge of the 59.54 keV photopeak at 44 keV is due to hole collection of the events occurring near the anode and the upper edge at 60 keV is due to electron collection of events near the cathode. As the thickness increases, the hole collection becomes increasingly worse until predominately one-carrier collection prevails (Figure 5) where some electron trapping has caused downshifting of the photopeaks. Figure 4 includes an experimental spectrum on a 1.1 mm thick detector. The experiment peak at 31 keV is a fluorescent iodine escape peak and is not included in the absorption processes of this model. The model only adds noise when an event is processed, so a strong electronics noise tail is not expected in the computed spectrum. The energies in keV and weights of the $^{241}Am$ source spectrum are[15,16] 11.89 (.0117); 13.9 (.1783); 17.8 (.1932); 20.8 (.0446); 26.35 (.0371); 59.54 (.5351). The major features in the computer generated plots are the relative peak heights, the peak positions and shapes, and the background below the peaks. All the figures are based on 50,000 absorbed photons.

The degradation of resolution caused by hole trapping in Figure 4 is emphasized by keeping all the parameters of Figure 4 constant and moving the source from the cathode to the anode. The resulting spectrum in Figure 6 is even a little optimistic compared to experimental results; the lower edge of the 59.54 keV photopeak at 6 keV is usually not seen experimentally.

Peaking of the electric field near the cathode in $HgI_2$ is suspected from photoconductivity observations.[4,14] Contact work function effects and the ionization of traps are likely explanations of the nonuniform electric fields. Recent measurements at our laboratory indicate substantial device polarization from distributed trap ionization in $HgI_2$. Figure 7($^{57}Co$) shows that a substantial background and low energy noise-like tail are the major effects of a linearly decreasing electric field. The energies in keV and weights of the $^{57}Co$ source are[15,16] 14.36 (.0897); 121.97 (.8087); 136.33 (.1016). The counting efficiency on the 121.97 keV photopeak has been greatly reduced by the nonuniform field since signal contribution from holes is greatly reduced. The electric field profile is intended to be a simple hypothetical case. Real electric field profiles might be expected to be somewhat parabolic with abrupt slope changes near the contacts.

Simulation of high energy performance has not yet been done. However, detector D19, which is well behaved and characterized in terms of agreement with calculated spectra (as in Figure 4), has been used to measure higher energy x-rays. Figure 8 shows the effect of increasing photon energy on resolution. Figure 9 shows the performance of D19 (1.1 mm thick) for $^{137}Cs$. The large low-energy tail is due to electron and Compton escape. The photopeak takes on the shape of a shelf which is to be expected for single-carrier collection when the total volume is uniformly irradiated.

Figure 10 shows the combined spectrum of $^{57}Co$ and $^{241}Am$, weighted 2:1 respectively, for CdTe with a nonuniform electric field. The field profile is shown schematically in the figure; the contact regions are effectively dead layers. The simulated dead layers are 75 um thick and are created by using a weak field region with 0.1 V/cm. The detector and electronic noise was 1020 rms electrons (10 keV FWHM) and $\tau_I = \tau_D = 0.1$ μsec. Only a rough comparison is intended between the experimental and computed spectra of Figure 10. The real detector has a planar contact and an opposite point contact geometry and the model implies a planar-planar contact geometry with its one-dimensional charge collection. If two-dimensional charge collection were employed in the model, then the computed peak-to-valley ratios would decrease and resemble the experimental values more closely.

Thus far, performance results for $HgI_2$ and CdTe for high energy photons is discouraging. The question is raised as to whether any high-Z semiconductor is of interest as a detector material. After a cursory examination of the known properties of binary semiconductors, one can speculate the existence of a material

most suitable for high-Z photon detection. The bandgap should be reasonably low to allow for the highest mobilities, but still greater than 1.5 eV to allow ambient operation. We have considered a hypothetically plausible material called Idealium with a bandgap of 1.7 eV, $\mu_e$ = 500 cm$^2$/V-sec, $\mu_h$ = 100 cm$^2$/V-sec, $\tau_e^+ = \tau_h^+$ = 1 μsec, and an effective Z similar to $HgI_2$. The simulated spectra of $^{57}Co$ with an Idealium detector are shown in Figures 11 and 12. Figure 11 is dominated by electron transport and looks fairly reasonable. Figure 12 is dominated by hole transport and shows considerably worse performance. For Idealium, $L_e$ = 5 cm, $L_h$ = 1 cm, and DL = 0.5 cm; thus, the problem of marginal two-carrier collection is very much evident in spite of its optimistic transport properties.

## Conclusions

Evaluation of high-Z semiconductors as spectrometers is difficult and uncertain in terms of determining actual performance limitations. To facilitate doing this, a detector x-ray spectrum simulation model has been developed and used to estimate transport properties by curve fitting, predict the performance of new materials, and optimize detector system performance for existing materials. The computed and experimental results indicate that where marginally low trapping lengths and/or mobilities prevail, a detector employing predominantly one-carrier collection may give the best results for certain photon energies. Under these circumstances, the results indicate that there may be nonorthodox approaches to making the detectors usable for some applications. The future for detection at higher photon energies is less clear since the relative penetration is deeper. This results in the necessity of efficient two-carrier collection as well as homogeneous transport properties.

## References


1. R. O. Bell, F. V. Wald, C. Canali, F. Nava, G. Ottaviani, IEEE Trans. Nucl. Sci., NS-21, No. 1, 331 (1974).
2. H. L. Malm, M. Martini, IEEE Trans. Nucl. Sci., NS-21, No. 1, 322 (1974).
3. K. Zanio, F. Krajenbrink, H. Montano, IEEE Trans. Nucl. Sci., NS-21, No. 1, 315 (1974).
4. S. P. Swierkowski, G. A. Armantrout, R. Wichner, *IEEE Trans. Nucl. Sci., NS-21, No. 1, 302 (1974).*
5. J. Llacer, M. K. Watt, M. Schieber, R. Carlston, W. Schnepple, IEEE Trans. Nucl. Sci., NS-21, No. 1, 305 (1974).
6. G. M. Martin, P. Bach, P. Guetin, Appl. Phys. Lett., 25, No. 5, 286 (1974).
7. J. P. Ponpon, R. Stuck, P. Siffert, C. Schwab, Nucl. Instr. and Meth., 119, 197 (1974).
8. R. H. Bube, Photoconductivity of Solids, John Wiley, New York, 1960.
9. T. A. McMath, M. Martini, Nucl. Instr. and Meth., 86, 245 (1970).
10. R. Trammel, F. J. Walter, Nucl. Instr. and Meth., 76, 317 (1969).
11. V. P. Katkov, A. I. Krupman, I. M. Taksar, Sov. Phys. Semicond., 7, No. 12, 1521 (1974).
12. M. J. Berger, "Monte-Carlo Calculations of the Penetration and Diffusion of Fast Charged Particles", in Methods in Computational Physics, Vol. 1, ed. B. Alder, Academic Press, New York, 1963.
13. M. Colbert, "SANDYL: A Computer Program for Calculating Combined Photon-Electron Transport in Complex Systems", Sandia Report SCL-DR-720109, March 1973.
14. R. H. Bube, Phys. Rev., 106, 703 (1957).
15. Table of Isotopes, 6th edition, ed. C. M. Lederer, John Wiley, New York, 1967.
16. H. R. Bowman, E. K. Hyde, S. G. Thompson, R. C. Jared, Science, 151, 562 (1966).


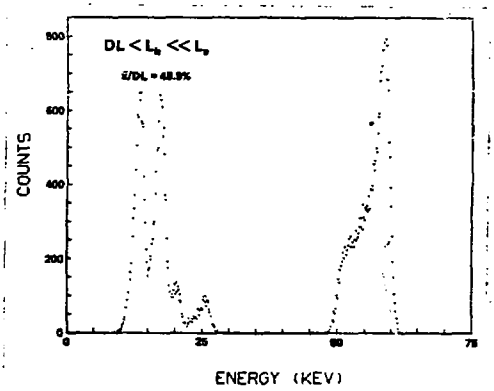


Fig. 1. Simulated $^{241}Am$ spectrum using 500 channels with the source incident on the cathode of $HgI_2$. The detector thickness is 35 μm. Figs. 1-5 are a series where all parameters are constant including the electric field and only the detector thickness (DL) changes.

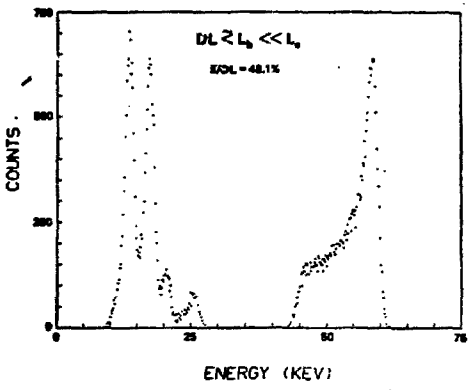


HGI2 AM241 -SPEC7 11/16/74
UE= 9.60E+01 TE= 5.00E-07 DL= 6.00E-03
UH= 3.00E+00 TH= 3.30E-07 V= 6.00E+01

Fig. 2. Simulated $^{241}Am$ spectrum with the source incident on the cathode of $HgI_2$. The detector thickness is 60 μm.

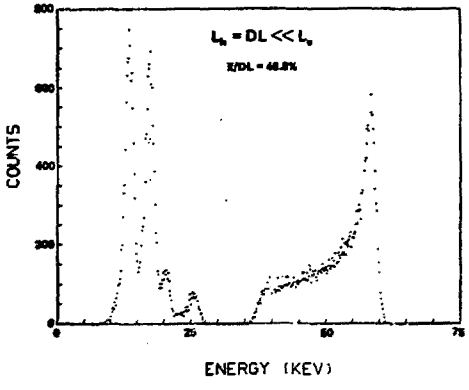


HGI2 AM241 -SPEC5 11/15/74
UE= 9.60E+01 TE= 5.00E-07 DL= 1.00E-02
UH= 3.00E+00 TH= 3.30E-07 V= 1.00E+02

Fig. 3. Simulated $^{241}Am$ spectrum with the source incident on the cathode of $HgI_2$. The detector thickness is 100 μm.

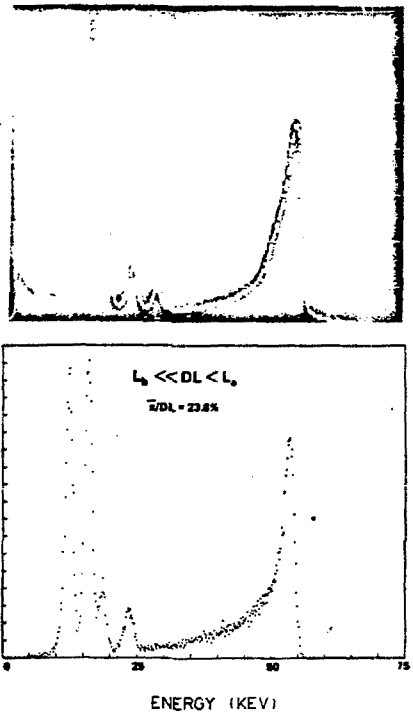


HGI2 AM241 -SPEC2 11/14/74
UE= 9.60E+01 TE= 5.00E-07 DL= 1.00E-01
UH= 3.00E+00 TH= 3.30E-07 V= 1.00E+03

Fig. 4. Simulated $^{241}Am$ spectrum with the source incident on the cathode of $HgI_2$ compared to an experimental spectrum taken with a detector 2x2x1.1 mm thick. The model detector is 1.0 mm thick.

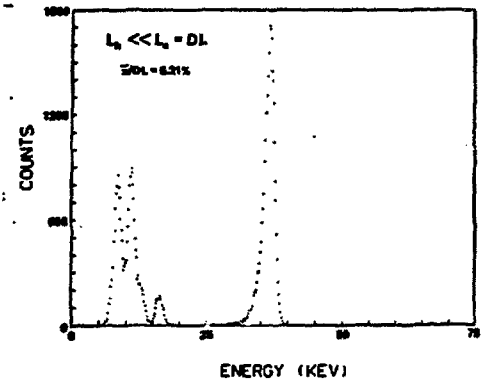


HGI2 AM241 -SPEC4 11/15/74
UE= 9.60E+01 TE= 5.00E-07 DL= 5.00E-01
UH= 3.00E+00 TH= 3.30E-07 V= 5.00E+03

Fig. 5. Simulated $^{241}Am$ spectrum with the source incident on the cathode of $HgI_2$. The detector thickness is 5.0 mm.

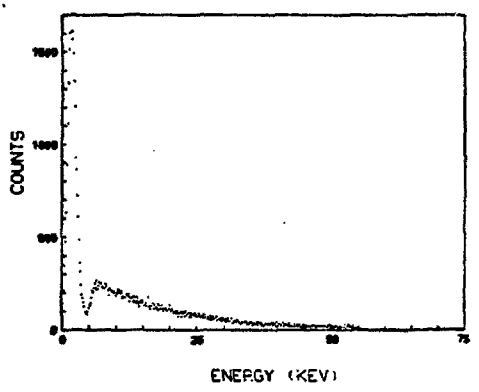


HGI2 AM241 -SPEC8 11/16/74
UE= 9.60E+01 TE= 5.00E-07 DL= 1.00E-01
UH= 3.00E+00 TH= 3.30E-07 V= 1.00E+03

Fig. 6. Simulated $^{241}Am$ spectrum with the source incident on the anode of $HgI_2$. The other parameters are unchanged from Fig. 4.

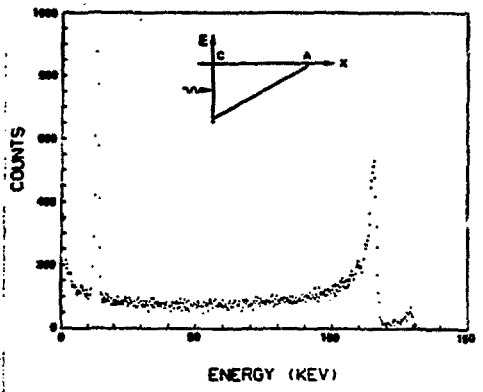


HGI2 C057 -SPEC11 E 11/16/74
UE= 9.60E+01 TE= 5.00E-07 DL= 1.00E-01
UH= 3.00E+00 TH= 3.30E-07 V= 1.01E+03

Fig. 7. Simulated $^{57}Co$ spectrum with the source incident on the cathode of $HgI_2$. The electric field profile is schematically shown.

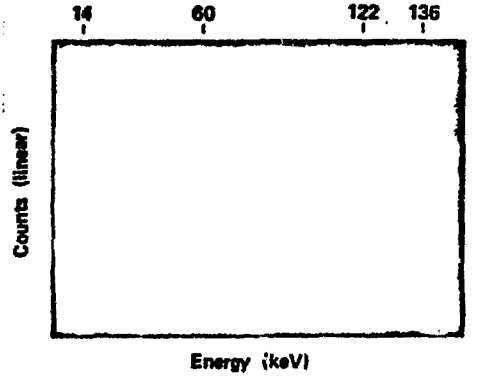


Fig. 8. $^{57}Co$ and $^{241}Am$ spectrum taken with $HgI_2$ detector D19(2x2x1.1 mm thick). The detector bias was 1 kV and the sources were incident on the cathode.

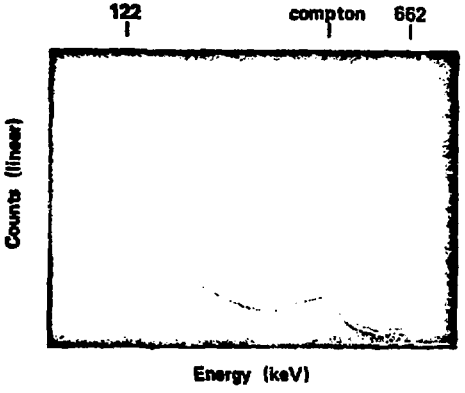


Fig. 9. $^{57}Co$ and $^{137}Cs$ spectrum taken with the sources incident on the cathode of $HgI_2$ detector D19.

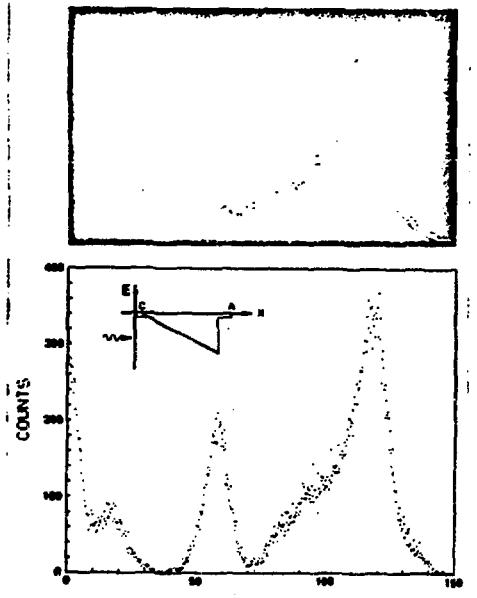


CDTE AM241C057 -SPEC18 E 11/20/74
UE= 1.00E+03 TE= 3.70E-08 DL= 1.50E-01
UH= 7.50E+01 TH= 3.20E-07 V= 9.10E+02

Fig. 10. Simulated spectrum of $^{57}Co$ and $^{241}Am$ with the sources incident on the cathode of CdTe. The experimental detector was partially collimated and had a thickness 1.5 mm and a bias of 850 volts.

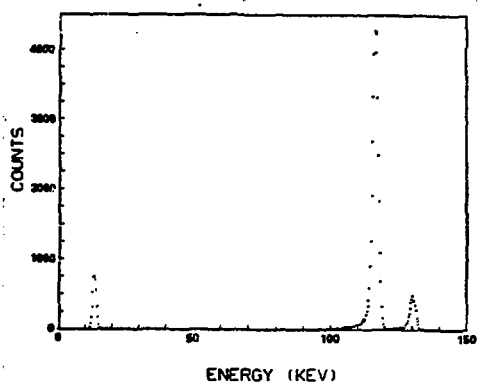


IDEALIUM C057 -SPEC19 11/20/74
UE= 5.00E+02 TE= 1.00E-06 DL= 5.00E-01
UH= 1.00E+02 TH= 1.00E-06 V= 5.00E+03

Fig. 11. Simulated spectrum of $^{57}Co$ with the source incident on the cathode of the hypothetical material Idealium.

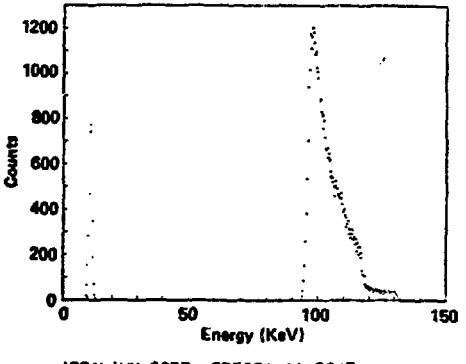


IDEALIUM C057 -SPEC21 11/20/74
UE= 5.00E+02 TE= 1.00E-06 DL= 5.00E-01
UH= 1.00E+02 TH= 1.00E-06 V= 5.00E+03

Fig. 12. Simulated spectrum of $^{57}Co$ with the source incident on the anode of the hypothetical material Idealium. The other parameters are unchanged from Fig. 11.